Vibrational Spectroscopy 80 (2015) 66–69

Contents lists available at ScienceDirect

Vibrational Spectroscopy

journal homepage: www.elsevier.com/locate/vibspec

Short communication

Raman and photoluminescence investigation of CdS/CdSe quantum dots on TiO_2 nanoparticles with multi-walled carbon nanotubes and their application in solar cells

Kun-Mu Lee[a,b], Sheng Hsiung Chang[a,*], Ming-Chung Wu[c], Chun-Guey Wu[a,d,**]

[a] Research Center for New Generation Photovoltaics, National Central University, Taoyuan 32001, Taiwan, ROC
[b] Department of Chemical and Material Engineering, National Central University, Taoyuan 32001, Taiwan, ROC
[c] Department of Chemical and Materials Engineering, Chang Gung University, Taoyuan 33302, Taiwan, ROC
[d] Department of Chemistry, National Central University, Taoyuan 32001, Taiwan, ROC

ARTICLE INFO

Article history:
Received 20 February 2015
Received in revised form 13 August 2015
Accepted 15 August 2015
Available online 20 August 2015

Keywords:
Energy transfer
Raman scattering
Photoluminescence

ABSTRACT

Raman spectroscopy and photoluminescence (PL) were used to investigate the improved short-circuit current density (J_{SC}) of CdS/CdSe quantum dot (QD)-sensitized solar cells with multi-walled carbon nanotubes (MWCNTs). Raman and PL experiments were carried out in order to explore the hot-electron and cold-electron injections, respectively. The experimental results showed that the concentration of MWCNTs influences the hot-electron and cold-electron injections from CdS/CdSe QDs to TiO_2 nanoparticles. Therefore, the improved J_{SC} in CdS/CdSe QD-sensitized solar cells can be explained as due to the better electron injections.

1. Introduction

Quantum dots have been widely used in solar cells to absorb the sunlight for photocurrent generation [1–4]. Time-resolved second harmonic spectroscopy has been used to demonstrate the efficient hot-electron injection from PbSe nanocrystals to TiO_2 nanoparticles [5]. Compared with the use of organic dyes in dye-sensitized solar cells (DSSCs), QDs present higher extinction coefficients [6], and their absorption bandgap can be adjusted by varying the size of the QDs due to the quantum confinement effect [7]. The fabrication process of QDs is also easier than that of organic dyes, which brings a benefit to reach the aim of low-cost solar energy. Cascade QDs have been used to increase the power conversion efficiency (PCE) of QD-SSCs, using materials such as CdS/CdTe, CdS/CdSe, ZnSe/CdSe, and ZnSe/CdSe/ZnSe [4,8–10]. TiO_2 nanoparticles [11,12] and ZnO nanostructures [1,2,4] have been widely used as photoanodes. The highest PCE of a QD-SSC is about 6.2% [4], but this is still far lower than the theoretical maximum PCE based on hot- (cold-) electron injection, which is about 43% (32%) [13,14]. Compared with the cold-electron injection from the conduction band of QDs to the Fermi level of the photoanode, the hot-electron injection takes place from QDs to the photoanode at the higher energy level, which results in a larger open-circuit voltage (V_{OC}). The PCE of the QD-SSCs is limited by the low fill factor (FF) due to charge carrier recombination originating from the surface defects of the porous photoanode [15]. The low FF results in a low V_{OC} and low J_{SC} [16]. For the photoanode electrode of QD-SSCs, the best way to reduce (increase) the charge carrier recombination (FF) is to increase the electron mobility of the photoanode by adding highly conductive materials such as carbon nanotubes (CNTs) [17], multi-walled carbon nanotubes (MWCNTs) [18], graphene [19], silver [20], and gold [21]. Static and dynamic photoluminescence quenching experiments have been performed to evaluate the efficiency of cold-electron injection from QDs to the photoanode [1,22,23]. However, efficient cold-electron injection from QDs to the photoanode cannot guarantee a high J_{SC} in QD-SSCs, because both hot-electron and cold-electron injections contribute to the generation of the photocurrent.

In this study, the MWCNTs were added to the TiO_2 nanoparticles to increase the PCE of CdS/CdSe QD-SSCs. Raman spectroscopy and photoluminescence (PL) were used to investigate the hot-electron and cold-electron injections from QDs to photoanode with and without MWCNTs, respectively.

2. Fabrication of TiO_2, TiO_2/MWCNT films and QD-SSC devices

The TiO_2 paste used for screen-printing in this study was prepared by mixing TiO_2 nanoparticles (P90), various concentrations of MWCNTs, ethyl cellulose (EC) and terpineol (anhydrous,

* Corresponding author. Fax: +886 3 4252 897.
** Corresponding author. Fax: +886 3 4252 897.
E-mail addresses: shchang@ncu.edu.tw (S.H. Chang), t610002@cc.ncu.eud.tw (C.-G. Wu).

http://dx.doi.org/10.1016/j.vibspec.2015.08.001
0924-2031/

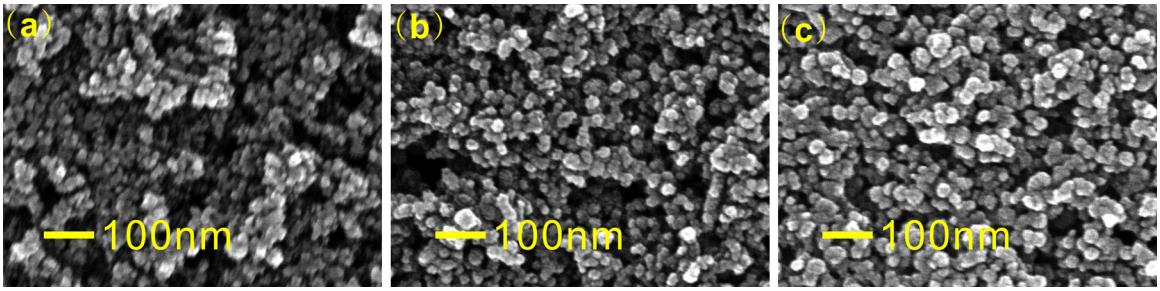

Fig. 1. (a), (b), and (c) show images of the surface morphology of TiO_2, CdS on TiO_2, and CdS/CdSe on TiO_2, respectively.

#86480, Fluka). The procedure is described in greater detail as follows: EC (5–15 mPas, #46070, Fluka) and EC (30–70 mPas, #46080, Fluka) were individually dissolved in ethanol to yield a 10 wt% solution, then 1.2 g EC (5–15) and 1.2 g EC (30–70) were added to a flask containing 1.2 g TiO_2 nanoparticles (using various concentrations of MWCNTs) and 2.5 terpineol. The paste mixture was dispersed in an ultrasonic bath and a rotary-evaporator was used to remove any residual ethanol or water from the mixture. The final TiO_2 paste formula was made with a three-roll mill (EXAKT E50). Screen-printing was used to prepare 4 μm thick TiO_2 samples with and without MWCNTs electrodes on fluorine-doped tin oxide (FTO) glass. The active area was fixed at 0.16 cm^2. The electrodes were then gradually heated under an O_2 gas flow at 450 °C for 30 min to remove any organic materials from the paste. After cooling to room temperature, the mesoporous TiO_2 electrodes (photoanodes) were then sequentially sensitized with CdS and CdSe QDs. The CdS layer was deposited on the photoanodes by the successive ion layer absorption and reaction (SILAR) process as previously reported. [24] The CdS loading could be controlled digitally by tuning the number of reaction cycles. Then, CdSe QDs were deposited on the TiO_2/CdS structure using the chemical bath deposition (CBD) method. [25] The loading of CdSe QDs can also be controlled by changing the number of reaction cycles. In these studies, two (three) reaction cycles of SILAR (CBD) were used for the deposition of CdS (CdSe). The QD-SSCs were sandwiched together with several parts. [1] Platinum-coated FTO counter electrodes were fabricated by electron-beam evaporation. The internal space of the TiO_2 electrodes and Pt counter electrodes was separated by a 60 μm thick hot melting spacer (Surlyn, DuPont), and was filled through a hole with polysulfide electrodes composed of 2 M Na_2S, 2 M S, 0.2 M KCl in a mixture of methanol and deionized water (7:3, v/v).

3. Measurements and characterizations

For evaluation of the current density–voltage (J–V) characteristics, a solar simulator (Yamashita Denso, YSS-50S) was used to irradiate the surface of the QD-SSCs, and the data were collected by a Keithley 2400 source meter. The intensity of the simulated sunlight was calibrated by an NREL-certificated Si solar cell (Oriel, 91150V) with a KG-5 filter to an intensity of 100 mW/cm^2 (AM 1.5G). The fabricated TiO_2 nanoparticles and CdS/CdSe QDs were analyzed by an ultra-high resolution electron microscope (UHR FE-SEM, HITACHI). The results of the hot (cold) electron injection from CdS/CdSe QDs to TiO_2 nanoparticles was investigated by a Raman spectroscopy (PL) using a commercial optical microscope system (UniRAM, Protrustech).

4. Results and discussion

Fig. 1 presents the surface morphology of the TiO_2, CdS on TiO_2, and CdSe/CdS on TiO_2. CdS and CdSe are coated on the surface of TiO_2 nanoparticles, which results in an increase in nanoparticle size as shown in Figs. 1(b) and (c).

The electron injection process is illustrated in Fig. 2. The photogenerated hot electrons in QDs can be injected into TiO_2 nanoparticles due to the long hot-electron lifetime (~1 ps) [26]. After the thermalization, the electrons relax to the conduction band of QD. Then, the cold electrons in QDs can be injected into

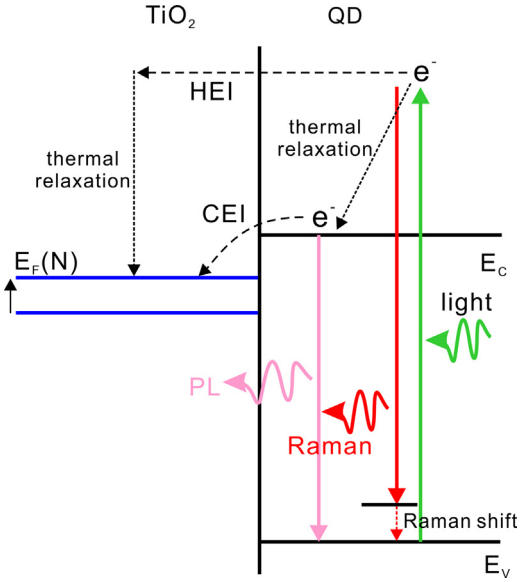

Fig. 2. Schematic view of the energy diagram at QD/TiO_2 interface. QD: quantum dot; E_F: Fermi level; E_C: conduction band; E_V: valence band; HEI: hot electron injection; CEI: cold electron injection. E_F of TiO_2 nanoparticles is proportional to the doping concentration (N).

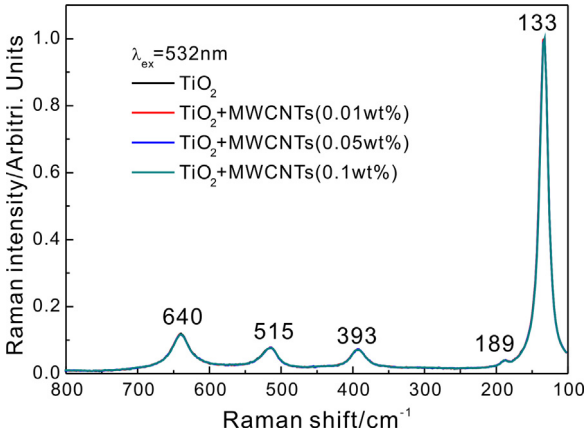

Fig. 3. Normalized Raman scattering of TiO_2 nanoparticles with different amounts of multi-walled carbon nanotubes.

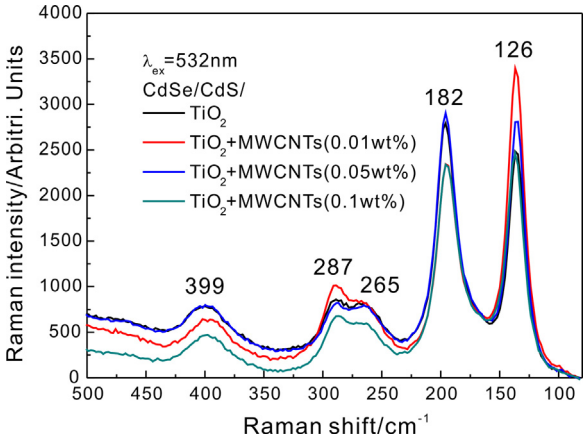

Fig. 4. Raman spectra of CdS/CdSe on TiO_2 nanoparticles with different amounts of multi-walled carbon nanotubes.

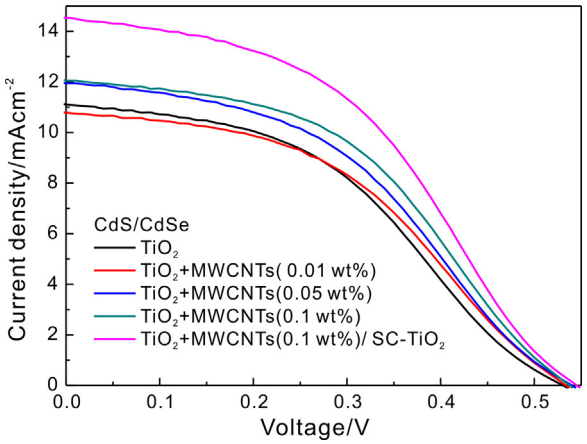

Fig. 6. *J–V* curves of CdS/CdSe quantum dot-sensitized solar cell under 1 sun illumination.

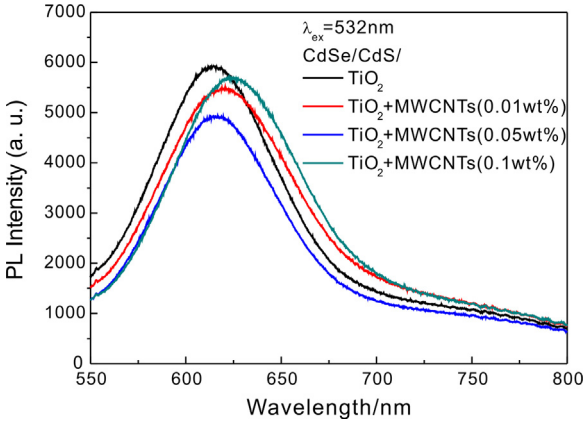

Fig. 5. Photoluminescence spectra of CdS/CdSe on TiO_2 nanoparticles with different amounts of multi-walled carbon nanotubes.

TiO_2 nanoparticles when the built-in electric potential ($= E_C - E_F(N)$) overcomes the electron–hole Coulomb potential (exciton binding energy) in QD. Therefore, both hot-electron and cold-electron injections contribute to the short-circuit current density of QD-SSC. PL quenching experiments have been used to investigate cold-electron injection from QDs to photoanode [1,23]. We think that the Raman quenching can be used to evaluate the hot-electron injection at QD/TiO_2 interface. In order to explore the correlation between the electron injections and the short-circuit current density of QD-SSC, the Raman and PL spectra of CdS/CdSe on TiO_2 nanoparticles were analyzed.

Fig. 3 presents the normalized Raman spectra of TiO_2 nanoparticles with different concentrations of MWCNTs under green light excitation (λ = 532 nm). The Raman fingerprints show that the TiO_2 nanoparticles are in anatase form [27]. The Ti—O vibrational modes of anatase TiO_2 are located at 393, 515, and 640 cm^{-1}. The Ti—Ti vibrational modes of anatase TiO_2 are located at 133 and 189 cm^{-1}. The four Raman spectra of the TiO_2 nanoparticles overlap well, which means that the microstructure of the TiO_2 nanoparticles has not been altered by the addition of MWCNTs. Fig. 4 presents the Raman spectra of CdS/CdSe on TiO_2 nanoparticles with different concentrations of MWCNTs under green light excitation (λ = 532 nm). The Raman shift of the lowest vibrational mode is a red-shift from 133 to 126 cm^{-1} following the deposition of CdS and CdSe on the surface of the TiO_2 nanoparticles, which means that the surface oxygen vacancies of TiO_2 nanoparticles are reduced [28]. The LO mode of CdS (CdSe) is located at 287 cm^{-1} (182 cm^{-1}). The CdS-like LO mode (265 cm^{-1}) can be attributed to the formation of a mixed CdS_xSe_{1-x} interfacial layer between the CdS and CdSe QDs [29] In the case of CdS/CdSe on TiO_2 nanoparticles, hot electrons can be injected from the CdSe to CdS to the TiO_2 nanoparticles if CdSe is not directly in touch with TiO_2. Therefore, the higher hot-electron injection from QDs to TiO_2 nanoparticles reduces the Raman intensities of CdS and CdSe. The oxygen vacancies in the TiO_2 nanoparticles and the Raman intensity of CdS both decrease with an increase in the MWCNTs concentration from 0.01 wt% to 0.1 wt%. Therefore, the efficiency of hot-electron injection from CdS to TiO_2 nanoparticles is increased due to the enhanced electron mobility in TiO_2 nanoparticles when the concentration of MWCNTs is increased from 0.01 wt% to 0.1 wt %. Fig. 5 presents the PL spectra of CdS/CdSe QDs on TiO_2 nanoparticles. Static PL quenching experiments have been used to evaluate the cold-electron injection from QDs to TiO_2 nanoparticles. [23] The lower PL intensity of the QDs corresponds to better cold-electron injection from QDs to TiO_2 nanoparticles. Therefore, it can be seen that the cold-electron injection from QDs to TiO_2 nanoparticles can be improved by adding the MWCNTs. The Fermi level of TiO_2 is also increased with increasing electron concentration [30,31], which results in a smaller energy difference between the conduction band of the CdS and the Fermi level of the TiO_2. The reduction of cold-electron injection can be explained by the smaller built-in electric field at the interface between CdS and TiO_2 when the concentration of MWCNTs is increased to 0.1 wt%. The Raman intensity and PL intensity are listed in Table 1.

Table 1
Raman intensity and photoluminescence intensity. The Raman intensity is obtained by removing the photoluminescence background.

CdS/CdSe	Peak intensity of oxygen vacancies	Peak intensity of CdSe	Peak intensity of CdS	Peak intensity of PL
meso-TiO_2	2464	2794	547	5903
meso-TiO_2 + MWCNTs (0.01 wt%)	3882	2342	804	5485
meso-TiO_2 + MWCNTs (0.05 wt%)	2801	2897	622	4934
meso-TiO_2 + MWCNTs (0.1 wt%)	2464	2342	619	5696

Table 2
Photovoltaic performances under 1 sun illumination (AM 1.5G, 100 mW/cm^2).

Photoanode	V_{oc} (V)	J_{sc} (mA/cm^2)	FF (%)	PCE (%)
meso-TiO_2	0.530	11.11	42.1	2.48 ± 0.3
meso-TiO_2 + MWCNTs (0.01 wt%)	0.533	10.78	43.4	2.50 ± 0.2
meso-TiO_2 + MWCNTs (0.05%)	0.542	11.95	42.2	2.72 ± 0.3
meso-TiO_2 + MWCNTs(0.1 wt%)	0.535	12.05	44.8	2.91 ± 0.3
meso-TiO_2 + MWCNTs (0.1 wt%)/SC-TiO_2	0.544	14.54	43.1	3.42 ± 0.2

Fig. 6 presents the *J–V* curves of the CdS/CdSe QD-sensitized solar cells. The photovoltaic performance results are listed in Table 2. The addition of MWCNTs significantly influences the photovoltaic performance in terms of J_{SC}. Compared with the reference solar cell (without MWCNTs), there is an improved J_{SC} which originates from the enhanced cold (hot) electron injection when the MWCNT concentration is 0.05 wt% (0.1 wt%). The addition of MWCNTs also slightly improves the FF from 42.1% to 44.8% when the doping concentration is increased to 0.1 wt%. In the case of TiO_2 nanoparticles with the addition of MWCNTs (0.1 wt%), the PCE of CdS/CdSe QD-SSC can be increased to 3.42% when a 3.5 μm-thick TiO_2 scattering layer is coated on the meso-TiO_2 layer to improve the light absorption.

5. Conclusions

In summary, we have successfully fabricated CdS/CdSe quantum dot-sensitized solar cells (QD-SSCs), which have a power conversion efficiency of 3.42%. The short-circuit current density (J_{SC}) can be increased by adding multi-walled carbon nanotubes (MWCNTs) into the TiO_2 photoanode. The Raman scattering and photoluminescence experiments provide clear evidences that the hot-electron injection and cold-electron injection from CdS/CdSe QDs to TiO_2 nanoparticles are enhanced when the concentration of MWCNTs is 0.1 wt% and 0.05 wt%, respectively. However, the hot electron-injection and cold-electron injection are not simultaneously enhanced when the concentration of MWCNTs is increased to 0.1 wt% due to the reduction in the built-in electric field at the interface between CdS and TiO_2. Therefore, there is a tradeoff between hot-electron injection and cold-electron injection from CdS/CdSe QDs to TiO_2 nanoparticles, which limits the J_{SC} in CdS/CdSe QD-SSCs. The best way is to increase the electron concentration of TiO_2 nanoparticles and to maintain the Fermi level of TiO_2 naoparticles for enhancing the J_{SC} in QD-SSCs.

Acknowledgments

This work was supported by the National Science Council under Grant NSC 101-2731-M-008-002-MY3. The devices fabrication was carried out in the Advanced Laboratory of Accommodation and Research for Organic Photovoltaics, Ministry of Science and Technology, Taiwan, ROC.

References

[1] H.-M. Cheng, K.-Y. Huang, K.-M. Lee, P. Yu, S.-C. Lin, J.-H. Huang, C.-G. Wu, J. Tang, Phys. Chem. Chem. Phys. 14 (2012) 13539–13548.
[2] C. Li, L. Yang, J. Xiao, Y.-C. Wu, M. Sodergaard, Y. Luo, D. Li, Q. Meng, B.B. Iversen, Phys. Chem. Chem. Phys. 15 (2013) 8710–8715.
[3] J.-W. Lee, D.-Y. Son, T.K. Ahn, H.-W. Shin, I.Y. Kim, S.-J. Hwang, M.J. Ko, S. Sui, H. Han, N.-G. Park, Sci. Rep. 3 (2013) 1050.
[4] K. Yan, L. Zhang, J. Qiu, Y. Qiu, Z. Zhu, J. Wang, S. Yang, J. Am. Chem. Soc. 135 (2013) 9531–9539.
[5] W.A. Tisdale, K.J. Williams, B.A. Timp, D.J. Norris, E.S. Aydil, X.-Y. Zhu, Science 328 (2010) 1543–1547.
[6] W.W. Yu, L. Qu, W. Guo, X. Peng, Chem. Mater. 15 (2003) 2854–2860.
[7] P.V. Kamat, J. Phys. Chem. C 112 (2008) 18373–18753.
[8] M.-J. Jin, X.-Y. Chen, Z.-M. Gao, T. Ling, X.-W. Du, Nanotechnology 23 (2012) 485401.
[9] Z. Zhu, J. Qiu, K. Yan, S. Yang, ACS Appl. Mater. Interfaces 5 (2013) 4000–4005.
[10] J. Xu, X. Yang, Q.-D. Yang, T.-L. Wong, S.-T. Lee, W.-J. Zhang, C.-S. Lee, J. Mater. Chem. 22 (2012) 13374–13379.
[11] I. Robel, V. Subramanian, M. Kuno, P.V. Kamat, J. Am. Chem. Soc. 128 (2006) 2385–2393.
[12] G.-Y. Lan, Z. Yang, Y.-W. Lin, Z.-H. Lin, H.-Y. Liao, H.-T. Chang, J. Mater. Chem. 19 (2009) 2349–2355.
[13] M.C. Bread, A.G. Midgett, M.C. Hanna, J.M. Luther, B.K. Hughes, A.J. Nozik, Nano Lett. 10 (2010) 3019–3027.
[14] W. Shockley, H.J. Queisser, J. Appl. Phys. 32 (1961) 510.
[15] Z. Zhang, J.T. Yates Jr., J. Phys. Chem. C 114 (2009) 3098–3101.
[16] Z. He, C. Zhong, X. Huang, W.-Y. Wong, H. Wu, L. Chen, S. Su, Y. Cao, Adv. Mater. 23 (2011) 4636–4643.
[17] K.T. Dembele, G.S. Selopal, C. Soldano, R. Nechache, J.C. Rimada, I. Concina, G. Sberveglieri, F. Rosei, A. Vomiero, J. Phys. Chem. C 117 (2013) 14510–14517.
[18] Y.-F. Chan, C.-C. Wang, B.-H. Chen, C.-Y. Chen, Prog. Photovoltaics: Res. Appl. 21 (2012) 47–57.
[19] S. Su, L. Gao, Y. Liu, Appl. Phys. Lett. 96 (2010) 083113.
[20] S.P. Lim, A. Pandikumar, N.M. Huang, H.N. Lim, G. Gu, T.L. Ma, RSC Adv. 4 (2014) 48236–48244.
[21] H. Hinsonti, W. Chomkitichai, A. Baba, N. Wetchakun, W. Kangwansupamonkon, S. Phanichphant, K. Shinbo, K. Kato, F. Kaneko, Int. J. Photoenergy 2014 (2014) 865423.
[22] T.-W. Zeng, I.-S. Liu, F.-C. Hsu, K.-T. Huang, H.-C. Liao, W.-F. Su, Opt. Express 18 (2010) A357–A365.
[23] K.-H. Lin, C.-Y. Chuang, Y.-Y. Lee, F.-C. Li, Y.-M. Chang, I.-P. Liu, S.-C. Chou, Y.-L. Lee, J. Phys. Chem. C 116 (2011) 1550–1555.
[24] H. Lee, H. Wang, P. Chen, D.R. Gamelin, S.M. Zakeeruddin, M. Gratzel, Md K. Nazeerudin, Nano Lett. 9 (2009) 4221–4227.
[25] M. Seol, H. Kim, Y. Tak, K. Yong, Chem. Commun. 46 (2010) 5521–5523.
[26] B.T. Spann, S.V. Bhat, Q. Nian, K.M. Rickey, G.J. Cheng, X. Ruan, X. Xu, Phys. Chem. Chem. Phys. 16 (2014) 10669–10678.
[27] W.F. Zhang, Y.L. He, M.S. Zhang, Z. Yin, Q. Chen, J. Phys. D: Appl. Phys. 33 (2000) 912.
[28] Z. Guo, O.V. Prezhdo, T. Hou, X. Chen, S.-T. Lee, Y. Li, J. Phys. Chem. Lett. 5 (2014) 1642–1647.
[29] S. Sfaelou, A.G. Knotos, P. Falaras, P. Lianos, J. Photochem. Photobiol. A: Chem. 275 (2014) 127–133.
[30] I. Mora-Sero, J. Bisquert, Nano Lett. 3 (2003) 945–949.
[31] R. Taziwa, E. Meyer, Adv. Nanoparticles 3 (2014) 54–63.